Desalination and Water Treatment
www.deswater.com
doi: 10.5004/dwt.2021.27713

237 (2021) 121–136
October

Performance and mechanism of nitrophenol removal by nano zero-valent iron supported on granular activated carbon

Jiankun Zhang*, Xueyang Zhang, Jiaqiang Liu, Linjun Zhang, Hong Zheng, Chengfang Yang

School of Environmental Engineering, Xuzhou University of Technology, Xuzhou 221111, China, emails: zhangjiankun@xzit.edu.cn (J.K. Zhang), zhangxy@163.com (X.Y. Zhang), 67727278@qq.com (J.Q. Liu), wole2009@yeah.net (L.J. Zhang), zhenghong670@163.com (H. Zheng), 155086526@qq.com (C.F. Yang)

Received 17 December 2020; Accepted 9 August 2021

ABSTRACT

Using granular activated carbon (GAC) as the carrier, a nano zero-valent iron composite (nZVI) was prepared by the liquid-phase reduction method. The surface morphology and element chemical morphology of nano zero-valent iron supported on granular activated carbon composite (nZVI/GAC) were characterized by X-ray photoelectron spectroscopy, X-ray diffraction, scanning electron microscopy, specific surface area and aperture analyzer (Brunauer–Emmett–Teller). The effects of different materials, initial concentration, initial pH, temperature and dosage of nZVI/GAC on the removal of nitrophenol were studied. The results show that the nano zero-valent iron is successfully supported on the granular activated carbon and showed spherical morphology, but the specific surface area and pore diameter of the activated carbon is reduced; the removal rate of p-nitrophenol by nZVI/GAC under acidic conditions is better than that under alkaline condition, and the removal rate of p-nitrophenol by nZVI/GAC increases with the increase of the dosage of nZVI/GAC and the decrease of the initial concentration of nitrophenol. In the process of nitrophenol removal, there is a synergism between the adsorption of activated carbon and the reduction and degradation of nanometer zero-valent iron. The data fitted the pseudo-second-order kinetic model well ($R^2 > 0.99$). To investigate the degradation pathway degradation products was analyzed by high-performance liquid chromatography-mass spectrometry.

Keywords: Granular activated carbon; Nanometer zero-valent iron; Nitrophenol; Synergism; Degradation

1. Introduction

Nitrophenol is an important and commonly used chemical raw material, which is widely used in the production of explosives, pharmaceuticals, pesticides, dyes, wood preservatives and rubber [1,2]. In the process of production and use, with the discharge of industrial wastewater, the environment will be polluted. Nitrophenol is a type of persistent pollutant with stable properties, high toxicity and three effects on the human body [3]. 2-nitrophenol, 4-nitrophenol and 2,4-dinitrophenol are listed in the list of priority control pollutants listed by the U.S. [4]. National Environmental Protection Agency and phenol pollutants are also listed as priority control pollutants in water bodies in China [5].

At present, there are various degradation technologies of nitrophenol, such as advanced oxidation processes [6], extraction [7], adsorption [8–10], reduction [11], biodegradation [12] and so on. Nano zero-valent iron (nZVI) compared to microscale ZVI has advantages such as large surface area, high and stable reactivity and consumption of low dosages. In addition, nZVI has been recently applied for in-situ and ex-situ remediation due to being non-toxic and cheap. [13,14]. However, nZVI is easy to oxidize and

* Corresponding author.

agglomerate, which limits its application [15]. Supporting nZVI on the carrier can improve its dispersion performance and reduce agglomeration [16]. In a further related study, Babaei et al. [14] show that the CS@nZVI provides very promising results for cost-effective treatment of wastewaters contaminated by Cd^{2+}, as well as high adsorption capacities, good and rapid separations and efficient technology for heavy metals removal. Ahmadi et al. [17] show that the nZVI@MWCNTs composite has a great potential for practical application for nitrate removal from aqueous solutions. Granular activated carbon (GAC) with respect to unique characteristics such as high surface areas, porous structure, and high adsorption capacity [18,19]. GAC is mostly used in the adsorption of a wide variety of water pollutants or in water treatment because of their ability to improve water by removing toxic materials [10,20]. Therefore, we choose the granular activated carbon as the carrier to support the nZVI onto the granular activated carbon, so that it has the excellent adsorption capacity of GAC and the strong reduction capacity of nZVI.

In this study, nitrophenol pollutants were used as the research object, granular activated carbon was used as the carrier, and the granular activated carbon-supported with nano zero-valent iron was prepared by liquid-phase reduction method [21], in order to make the nanometer zero-valent iron have better stability and dispersion, and can reduce and degrade pollutants efficiently. The structural characteristics of zero-valent iron nanoparticles supported on granular activated carbon were characterized by scanning electron microscopy (SEM), nitrogen adsorption–desorption, energy-dispersive X-ray spectroscopy, X-ray diffraction (XRD) and X-ray photoelectron spectroscopy (XPS). By analyzing the Fourier-transform infrared (FTIR) spectrum, X-ray photoelectron spectroscopy and high-performance liquid chromatography-mass spectrometry (HPLC-MS) of granular activated carbon-supported nano zero-valent iron material, the degradation products and degradation paths of nitrophenol were analyzed.

2. Materials and methods

2.1. Materials and instruments

The reagents used in the experiment are: sodium borohydride ($NaBH_4$), ferrous sulfate heptahydrate ($FeSO_4{\cdot}7H_2O$), granular activated carbon (GAC), concentrated sulfuric acid (H_2SO_4), hydrochloric acid (HCl), polyethylene glycol (PEG4000), anhydrous ethanol (C_2H_6O), acetone (CH_3COCH_3) are all analytical pure, purchased in Fuchen (Tianjin) Chemical Reagent Co., Ltd., and the experimental water is deionized water.

2.2. Preparation of materials

Granular activated carbon was immersed in 1 mol/L hydrochloric acid for 24 h, then cleaned with deionized water, then immersed in absolute ethanol for 8 h, and dried by blowing at 105°C. Weigh polyethylene glycol to dissolve in anhydrous ethanol, then weigh a certain amount of $FeSO_4{\cdot}7H_2O$ to dissolve in deionized water, add it into a three-port flask, and add a certain amount of pretreated active carbon. Before the reaction, nitrogen is introduced to remove the dissolved oxygen, and 0.45 mol/L $NaBH_4$ solution is added slowly. After the $NaBH_4$ solution is added, continue to inject nitrogen and stir for 30 min. After the reaction, the composite materials in three flasks were washed three times with anaerobic water, one time with anhydrous ethanol, three times with acetone, and then dried at 70°C in a vacuum drying oven to obtain nZVI/GAC particles. Granular activated carbon is not added during the preparation of nano zero-valent iron, and the remaining methods are the same as the above process.

2.3. Characterization of materials

The specific surface area and pore size of nano zero-valent iron supported on granular activated carbon and granular activated carbon were measured at 77.298 K by using the automatic surface area and pore size analyzer (Kubo-X1000, China). Scanning electron microscopy (Su8020, Japan) was used to analyze the surface morphology of granular activated carbon-supported with nano zero-valent iron. X-ray diffractometer (X'Pert PRO MPD, Netherlands) was used to compare and analyze the changes of the surface crystal composition of granular activated carbon before and after supporting nano zero-valent iron. X-ray photoelectron spectroscopy (ESCALAB 250XI, USA) was used to analyze the elements and valence states in the materials. The changes of functional groups on the surface of granular activated carbon before and after supporting nano zero-valent iron were analyzed by Fourier-transform infrared spectrometer (Nicolet iS10, USA).

2.4. Experimental methods

During the experiment, the solution was placed in a 500 mL reagent bottle. The flask was sealed and stirred in a temperature-controlled water bath oscillator (SHA-B, Shanghai, China) at 200 rpm and 25°C. Unless otherwise specified, the concentration of the reagent was 200 mg/L and the dosage of the material was 2 g. The temperature is controlled by adjusting the water bath temperature of the oscillator (20°C, 30°C, and 40°C), the pH of the solution is adjusted to between 2.0 and 11.0 with 0.1 mol/L NaOH or 0.1 mol/L HCl, and measured with a pH meter (pH-3c type, Shanghai). In order to study the effect of nZVI/GAC dosage on the removal rate of O-nitrophenol (ONP), P-nitrophenol (PNP), 2,4-dinitrophenol (2,4-DNP), different dosages (0.5, 1.5, 2, 2.5, 3, and 3.5 g) were tested. The experimental methods is shown in Table 1.

2.5. Analysis method

High-performance liquid chromatography (P1201, Dalian Elite) was used to determine the target pollutants and their corresponding degradation products in wastewater. Before sample analysis, filter with 0.45 μm and use the waters reverse C18 column for the chromatographic column. The test conditions are as follows: column temperature is 30°C, the flow rate is 1.0 mL/min, UV detector wavelength of 10 μl o-nitrophenol is 279 nm, the ratio of water to methanol is 0.30:0.70; UV detector wavelength of p-nitrophenol is 319 nm, ratio of water to methanol is 0.45:0.55; UV detector

wavelength of 2,4-dinitrophenol is 260 nm, ratio of water to methanol is 0.40:0.60. The intermediate products produced in the reaction process were determined by liquid chromatography-mass spectrometry (Waters 2695). Methanol and water were used as mobile phase, the ratio was 1:1, the flow rate was 0.2 mL/min, the ion source was ESI, the ratio of mass to charge was 50–500, and the capillary voltage was 4 keV. All analytical experiments were repeated twice and the average values are reported.

3. Results and discussion

3.1. Characteristic analysis of materials

3.1.1. Analysis of surface groups

The FT-IR spectrum of activated carbon-supported nano iron and granular activated carbon is shown in Fig. 1. It can be seen from the analysis spectrum that the peak of granular activated carbon-supported nano zero-valent iron particles at wavenumbers 469.80 and 529.12 cm^{-1} is the expansion vibration peak of Fe–O on Fe_2O_3 and Fe_3O_4 formed by oxidation [22], and the peak at wavenumbers 830.27 and 900.75 cm^{-1} is caused by the deformation vibration of hydroxyl in the iron hydroxide formed during the preparation of materials. The absorption peaks of GAC and nZVI/GAC at wavenumbers of 1,560.44; 1,622.12 and 1,732.51 cm^{-1} are all the characteristic peaks caused by C=C and C–O–C corresponding to the functional groups on the surface of activated carbon [23], so it can be seen that the granular activated carbon particles supported with nano zero-valent iron materials retain the original characteristic functional groups of activated carbon, which also shows that the surface functional groups of granular activated carbon were almost unchanged after supported nano zero-valent iron.

3.1.2. Specific surface area and pore size analysis

The N_2 adsorption/desorption curve and pore size distribution of granular activated carbon-supported nano iron and granular activated carbon are given in Fig. 2a. It can be seen that the N_2 adsorption/desorption isotherms of GAC and nZVI/GAC are of type I, which are typical Langmuir isotherms. Fig. 2b shows the mesoporous analysis of materials by the Barrett–Joyner–Halenda method. Pore size distribution of GAC and nZVI/GAC is mainly concentrated in the range of 3–5 nm. Fig. 2c shows the micropore analysis of materials by the Horvaih–Kawazoe (H–K) method. Pore size distribution of GAC and nZVI/GAC is mainly concentrated in the range of 0.5–0.6 nm. The specific surface area and pore diameter of the granular activated carbon-supported with nano zero-valent iron are respectively 961.85 m^2/g and 2.35 nm, 807.58 m^2/g and 2.26 nm. The specific surface area and pore diameter of the granular activated carbon-supported with nano iron is smaller than those of the granular activated carbon without nano iron, which is mainly due to the fact that the nano iron particles occupy the adsorption site and part of the pores of the granular activated carbon [24].

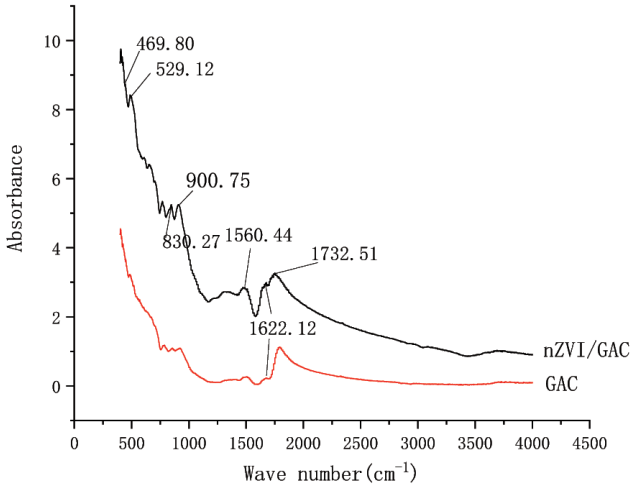

Fig. 1. FTIR spectrum of nanometer zero-valent iron supported on granular activated carbon.

3.1.3. Surface morphology analysis

SEM characterization of GAC, nZVI/GAC and nZVI were carried out. Fig. 3 is the SEM map of each material. From Fig. 3a and b, it can be seen that the pore structure of the unsupported activated carbon is developed, evenly distributed, and the pore channel is obvious; from Fig. 3c and d it can be seen that the activated carbon-supported with nano iron particles is partially supported on the surface of the granular activated carbon, and partially supported into the pore of the activated carbon. There are black particles on the surface of activated carbon-supported with nano iron, and the size of these black particles is relatively uniform. The results of SEM analysis show that the nano iron supported on the activated carbon does not agglomerate, which increases the activity of the nano iron material, and improves the efficiency of pollution removal by compounding with the activated carbon. As can be observed in Fig. 3e and f, the agglomeration of unsupported nano iron is serious.

3.1.4. Crystal structure analysis

XRD diffraction patterns of granular activated carbon, nano zero-valent iron, and nano iron supported on activated carbon are shown in Fig. 4. The Fe^0 characteristic peak appears at $2\theta = 42°–44°$, but the relative width of the diffraction peak is weak and wide dispersion, while the intensity of the diffraction peak of nano zero-valent iron is high and sharp [25]. This shows that nano zero-valent iron adheres to or enters the surface of granular activated carbon. However, the amount of nano zero-valent iron is far less than that of nano zero-valent iron alone. There are some fine peaks at about $2\theta = 35°$ and 26° which are iron oxides, indicating that part of the zero-valent iron supported on the activated carbon is oxidized to Fe_2O_3, Fe_3O_4 and FeOOH. The diffraction peak of amorphous carbon appeared in the range of $2\theta = 22°$, but the peak of supported nano iron activated carbon was weaker than that of activated carbon. One is that the supported nano zero-valent activated carbon had nZVI material supported on

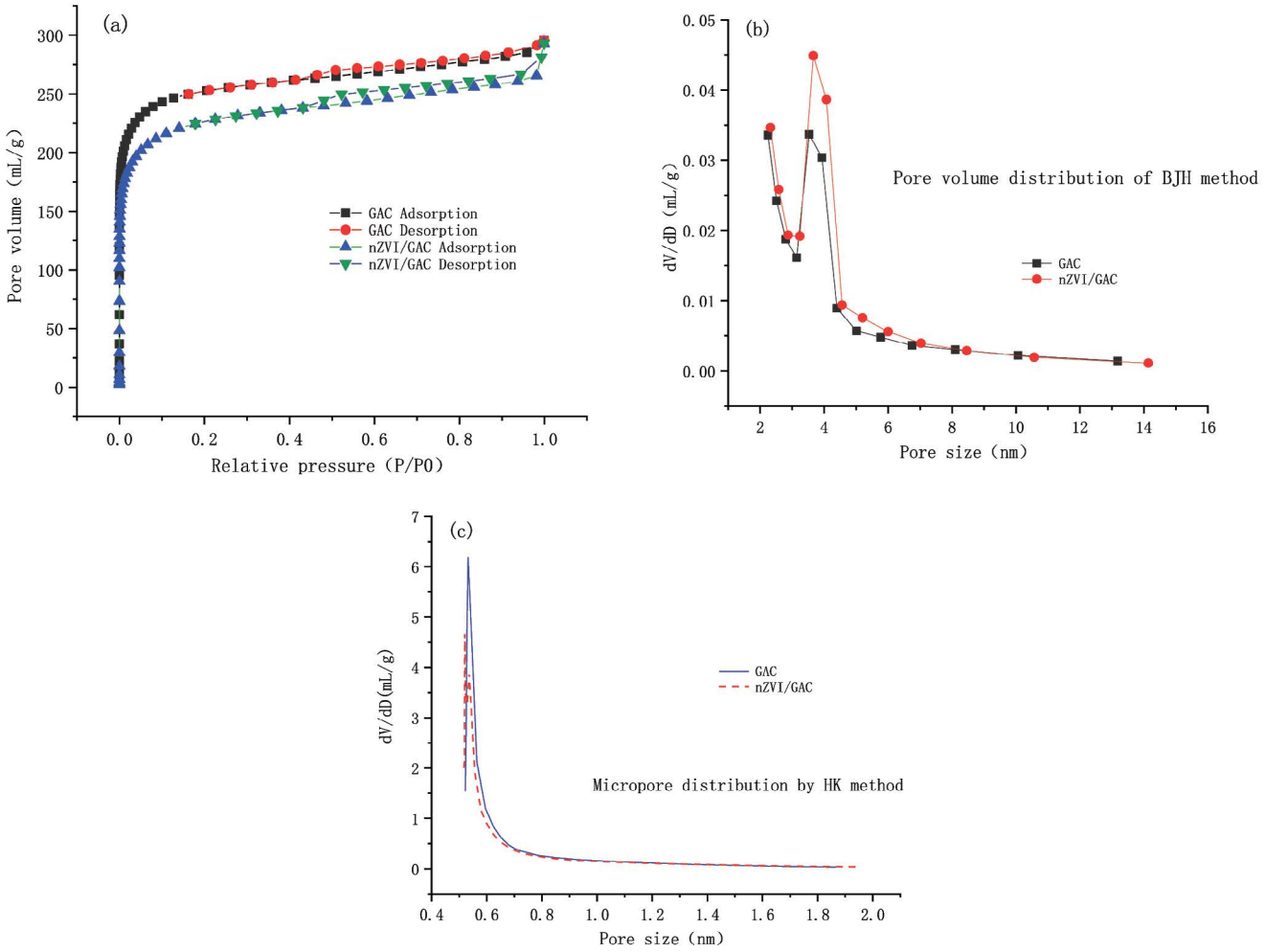

Fig. 2. N_2 adsorption/desorption curves and pore size distributions of GAC and nZVI/GAC materials (a) adsorption–desorption isotherms, (b) Barrett–Joyner–Halenda pore size distribution and (c) Horvaih–Kawazoe (H–K) micropore distribution.

the activated carbon, and the other is that some pores of the activated carbon collapsed due to the agitation during the supporting process [26]. Comply with nZVI standard card JCPDS No.06–696.

3.1.5. XPS analysis

XPS spectrum of nZVI/GAC material is shown in Fig. 5. Fig. 5a is the full spectrum scanning diagram of the material. Combined with the test results in Fig. 5b–d, we can see that there are C, Fe, O and other characteristic peaks, indicating that the surface of the material is mainly composed of these three elements. Fig. 5c shows the map of O1s XPS, with the largest peak value at 532.7eV, mainly forming Fe_2O_3. The map range is between 529.5 and 535.5 eV, mainly including the binding energy of O^{2-}, oh and adsorbed water molecules. Fig. 5d is the map of Fe2p XPS. There are two large peaks in 711 and 724.9 eV respectively, mainly the oxides of Fe^{2+} and Fe^{3+} [27]. This is due to the oxidation of zero-valent iron in the air of nZVI/GAC, which is zero-valent iron at 704.5 eV.

3.2. Removal of nitrophenol

3.2.1. Effect of different materials on PNP removal

The removal effect of different materials on PNP is illustrated in Fig. 6. It can be observed that the order of PNP adsorption and degradation capacity is nZVI/GAC > GAC > nZVI. With the increase of time, the removal rate of p-nitrophenol of three different materials gradually increased, and the removal rate of nZVI/GAC material gradually stabilized after 60 min. The specific surface area of the activated carbon-supported with nano iron is smaller than that of the non-supported activated carbon, and the content of nano iron supported on the activated carbon is also smaller than that of the single nano iron, but nZVI/GAC has the best removal effect on p-nitrophenol, and the removal rate is about 97%. In the initial stage of p-nitrophenol removal by nZVI/GAC, due to the adsorption of granular activated carbon, the removal rate of PNP was faster. When the adsorption sites of granular activated carbon were gradually occupied, nZVI supported on granular activated carbon continued to react with nitrophenol.

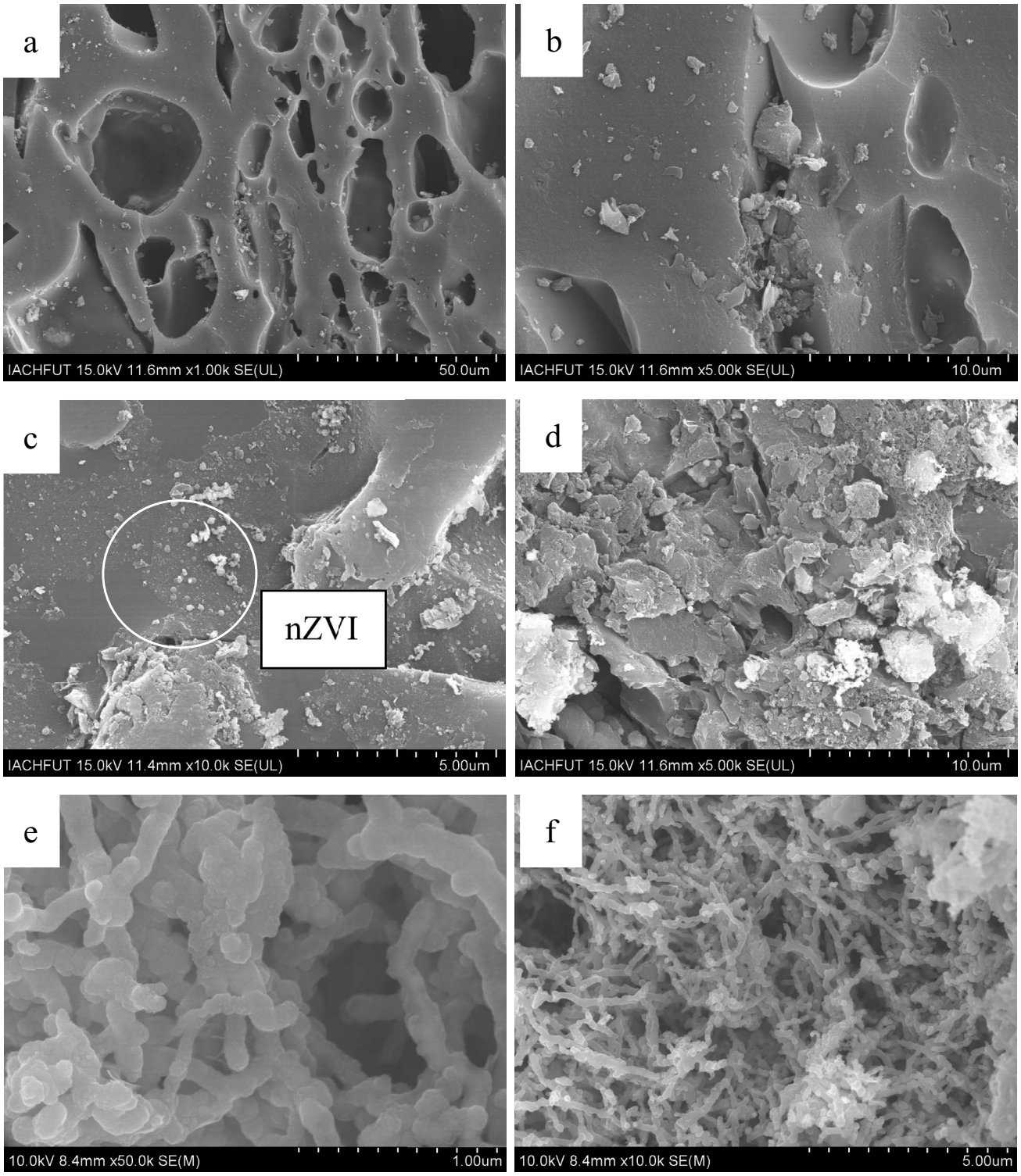

Fig. 3. SEM maps of GAC and nZVI/GAC (a, b) GAC; (c, d) nZVI/GAC and (e, f) nZVI.

There was a synergistic effect between activated carbon and nano zero-valent iron. Compared with GAC and nZVI alone, the removal efficiency of nZVI/GAC was the highest [28]. However, after the adsorption of activated carbon alone is saturated, the adsorption reaches equilibrium, and the removal rate is relatively stable. The nano zero-valent iron alone is easy to agglomerate, which is not conducive to the mass transfer with the target pollutant, and there is oxidation phenomenon in the preparation and transfer process, resulting in the removal rate of PNP lower than nZVI/

GAC. Compared with nZVI, GAC had a higher removal rate of PNP at the beginning of the reaction. With the extension of reaction time, the adsorption of PNP by GAC gradually reached saturation, reaching 95% of the adsorption

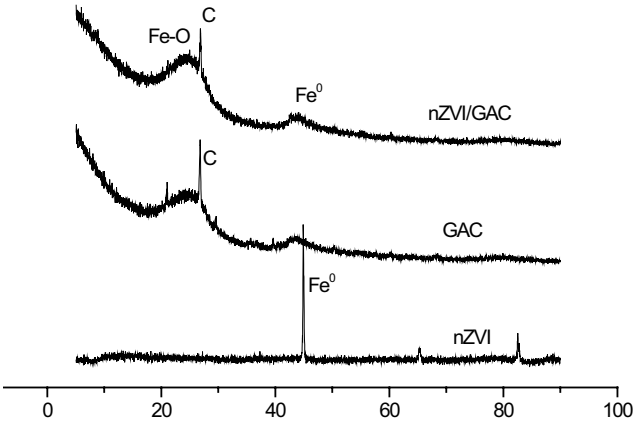

Fig. 4. XRD patterns of GAC, nZVI and nZVI/GAC.

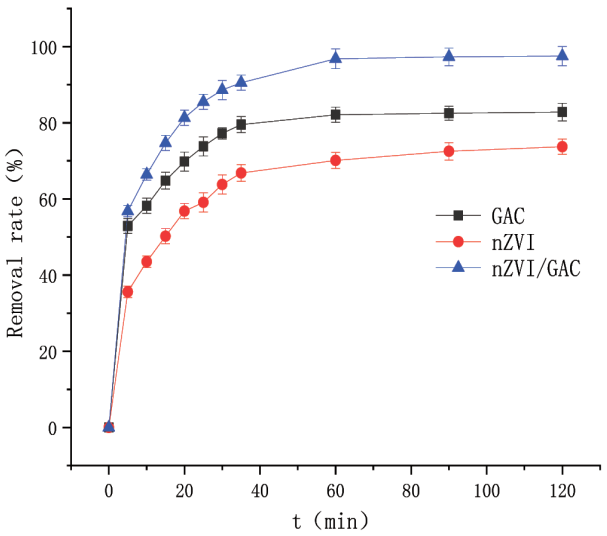

Fig. 6. Effects of different materials on the removal of p-nitrophenol.

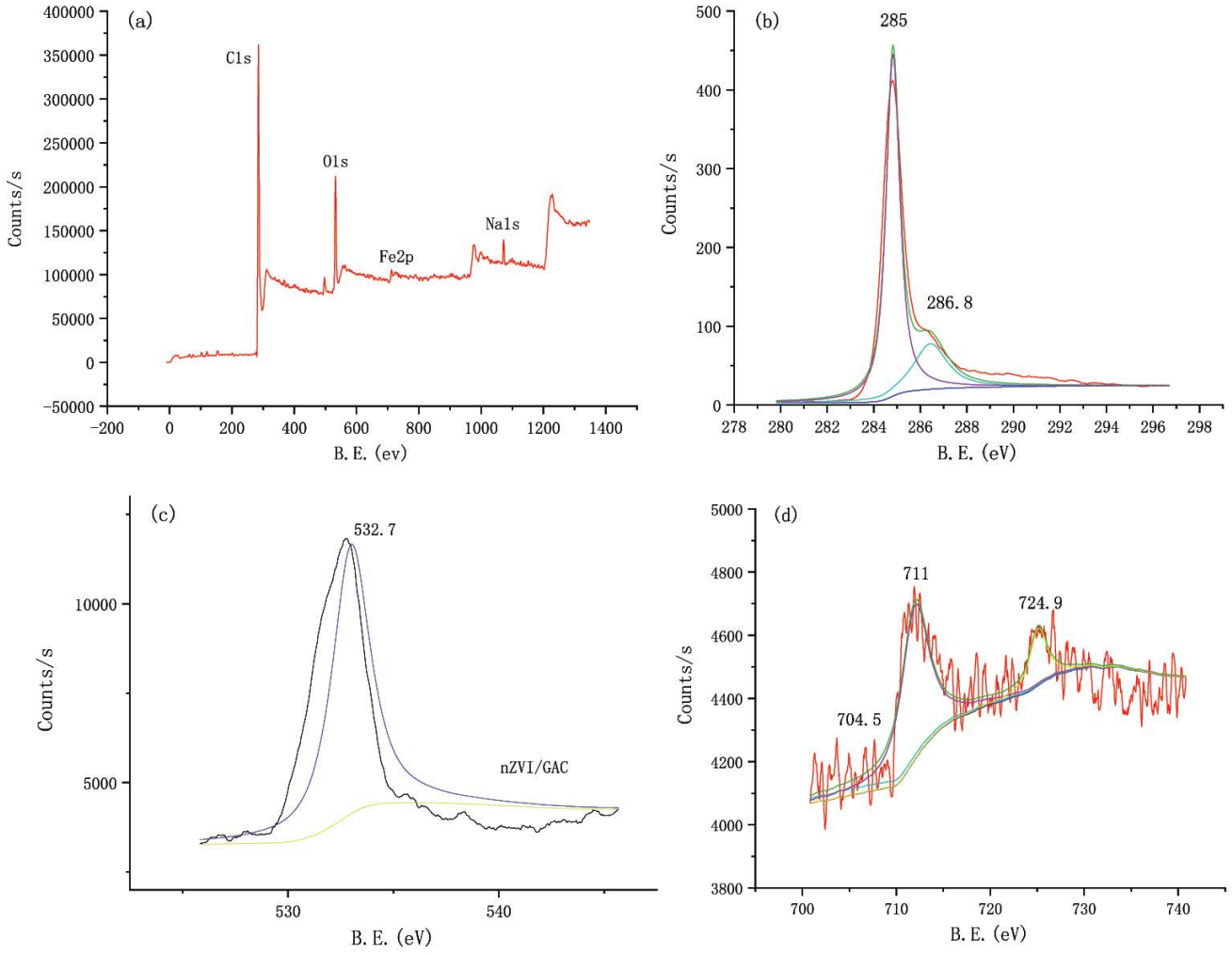

Fig. 5. XPS atlas of nZVI/GAC (a) nZVI/GAC full scan, (b) nZVI/GAC C, (c) nZVI/GAC O and (d) nZVI/GAC Fe.

equilibrium at 30 min and reaching saturation at 60 min. The removal rate of nZVI was over 70% in 120 min.

3.2.2. Effect of dosage

The effect of the dosage of nZVI/GAC on the reductive degradation of nitrophenol is illustrated in Fig. 7. The removal of ONP, PNP and 2,4-DNP increases with the increase of the dosage of nZVI/GAC. When the dosage increased from 0.5 to 3.5 g/L, the removal rates of ONP, PNP, 2,4-DNP increased from 75.42%, 70.38%, 68.62% to 98.40%, 97.82% and 94.35%, respectively. This is because, with the increase of the amount of nano zero-valent iron supported on the activated carbon, the amount of activated carbon and the amount of nZVI is increased, which makes the contact opportunity between iron and target pollutants increase, and the adsorption point provided by the activated carbon is also increased, so the removal rate is increased. Nitrophenols are adsorbed on the active sites by activated carbon and then reduced by nano zero-valent iron supported on the surface of activated carbon [29]. Secondly, because the nitro group on the benzene ring is electron absorption group, the more nitro substituents are, the more difficult nitroarene is to degrade; therefore, in Fig. 7 it can be seen that the removal rate of ONP and PNP is almost the same, but both are higher than 2,4-DNP. When the dosage is more than 2 g/L, and the dosage is further increased, the degradation rate of nitrophenols does not increase significantly.

3.2.3. Effect of pH

Fig. 8 shows the degradation curve of nitrophenol removed by nZVI/GAC with pH in the range of 2–11. PH is an important factor affecting the removal of nitrophenol by nZVI/GAC. It can be seen that the removal efficiency of nZVI/GAC to ONP, PNP and 2,4-DNP decreased gradually with the increase of pH. The removal rate of DNP has little change in the range of pH 2–3. When the pH is greater than 3, the removal rate decreases significantly. When the pH is in the range of 7–11, the removal rate of DNP has no significant change. When the pH is greater than 7, the removal rates of ONP and PNP decrease significantly. Because there are a lot of H^+ in the solution under the condition of low initial pH value, H^+ can maintain the surface-active reaction site of nZVI, promote the loss of electrons of zero-valent iron, and promote the reduction and degradation of nitrophenols by nZVI/GAC. Lee et al. [30] showed that the degradation of nitrate by nZVI is an acid-driven process. When the pH is alkaline, the OH^- in the solution makes the surface of nZVI form iron hydroxide, and passivation occurs, which reduces the surface-active reaction site of nZVI and affects the removal of p-nitrophenols.

3.2.4. Effect of reaction time

It can be seen from Fig. 9 that the removal of three nitrophenols by nZVI/GAC shows a similar trend with the

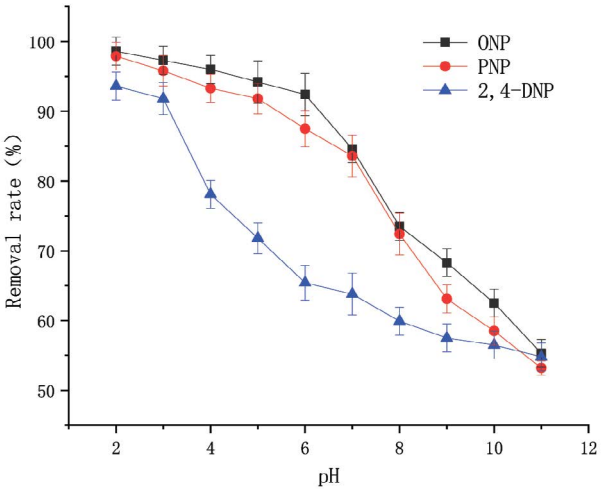

Fig. 8. Effect of pH on removal of nitrophenol by nZVI/GAC.

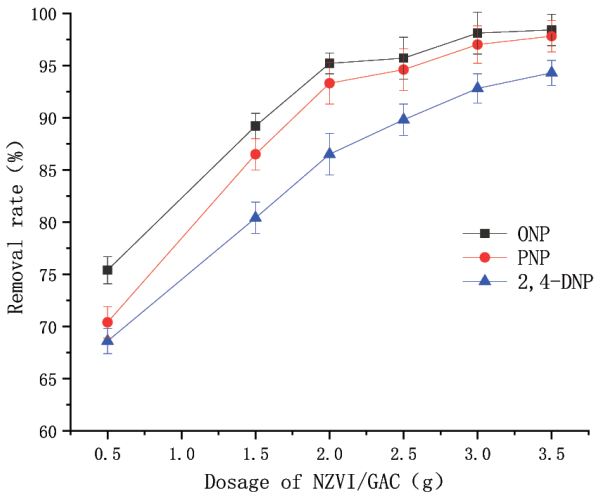

Fig. 7. Effect of nZVI/GAC dosage on nitrophenol removal.

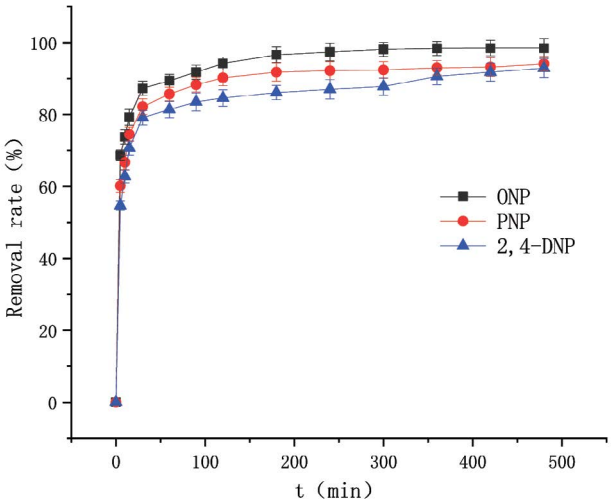

Fig. 9. Effect of reaction time on removal of nitrophenol by nZVI/GAC.

extension of reaction time. In the first 5 min of the reaction, the removal rate was over 55%. There was a synergistic effect between activated carbon and nano zero-valent iron particles, which improved the removal rate. The removal rates of ONP, PNP and 2,4-DNP were 88%, 82.9% and 79.5% respectively in 30 min. The removal rate of ONP reached 90% at 60 min and increased slowly at 240 min. In the initial stage, due to a large number of adsorption sites on the GAC surface and a large number of active nZVI particles, the removal rate of the target pollutants is relatively high under the adsorption of active carbon and the reduction of nZVI. With the progress of the reaction, the adsorption pores in nZVI/GAC particles are gradually occupied and reduced, reducing the adsorption capacity of the target pollutants, which leads to the decrease of the contact chance between nitrophenol and nZVI particles, and with the reduction of nitrophenol, nZVI loses its activity and removal rate gradually.

3.2.5. Effect of reaction temperature

The effect of temperature on the removal of nitrophenol by nZVI/GAC is illustrated in Fig. 10. The removal rate increases with the increase of reaction temperature. The effect of temperature on the adsorption of activated carbon is mainly attributable to the heat of adsorption. Most of the adsorption processes are exothermic. The increase in temperature will reduce the adsorption amount and the removal rate. However, the removal of nitrophenol by nZVI/GAC particles, in addition to the adsorption of activated carbon, is also due to the reduction of nZVI In this way, the reaction is mainly a chemical reaction, and the increase of temperature is conducive to the reaction [31], the migration of nitrophenol in solution, the contact probability of nitrophenol and nZVI/GAC, and the active energy and surface binding of electronic migration of nZVI/GAC.

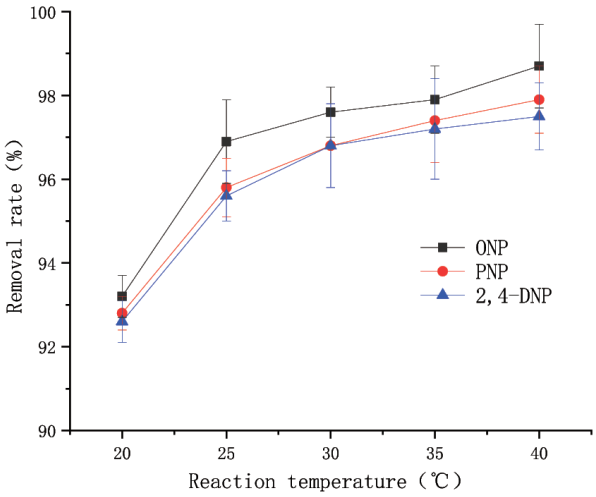

Fig. 10. Effect of temperature on nitrophenol removal by nZVI/GAC.

3.2.6. Effect of initial concentration

Fig. 11 shows the curve of the removal of nitrophenol by nZVI/GAC at different initial concentrations. With the increase of the initial concentration of nitrophenol, the degradation rate of the three nitrophenols decreased. The removal rates of ONP, PNP and 2,4-DNP increased from 50 to 500 mg/L, respectively, from 99.2% to 83.3%, 99.1% to 79.7%, 97.8% to 71.4%. It can be seen that the initial concentration have a certain influence on the reduction efficiency of nZVI/GAC. With the increase of nitrophenol concentration, the degradation efficiency gradually decreases. This is because the active sites on nZVI/GAC are limited. The higher pollutant concentration can promote their combination with the active sites, and the contact probability with nZVI will increase. As the reaction proceeds, the adsorption sites are occupied, and the oxides and hydroxides of iron are formed in nZVI materials, resulting in the passivation of the surface of nZVI and reducing the removal rate.

The solution with a high initial concentration has high adsorption capacity, but the removal rate is reduced. Because of the increase of initial mass concentration, the total amount of ONP, PNP, 2,4-DNP in the solution system

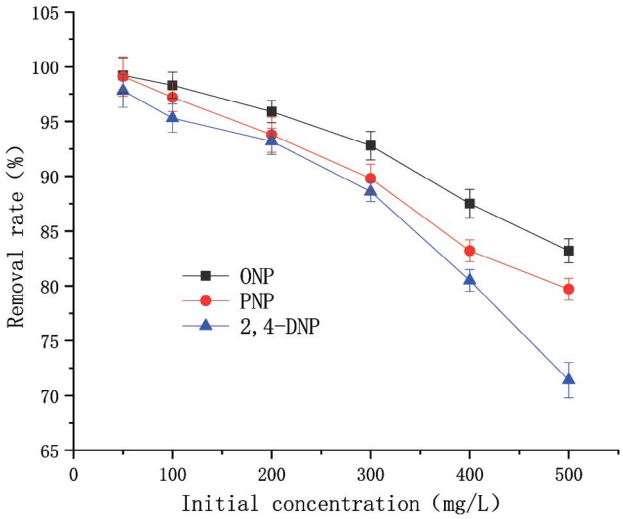

Fig. 11. Effect of initial concentration on nitrophenol removal by nZVI/GAC.

is increased substantially. When the adsorption capacity of nZVI/GAC reaches or approaches the adsorption capacity of the adsorbent, more nitrophenols in the solution will not be adsorbed and degraded by nZVI/GAC.

3.2.7. Effect of dissolved oxygen

Nitrogen and oxygen were injected into a conical flask to investigate the effect of oxygen on the reduction of nitrophenol by nZVI/GAC. The dissolved oxygen solubility was controlled at 6 mg/L, the reaction time was 60 min, and 2.0 g nZVI/GAC was added.

The effect of oxygen on the removal rate of nitrophenol is shown in Fig. 12. It can be seen from Fig. 12 that oxygen has a definite inhibitory effect on the degradation of nitrophenol by nZVI/GAC. This is because oxygen in the water will react with nano zero-valent iron as follows:

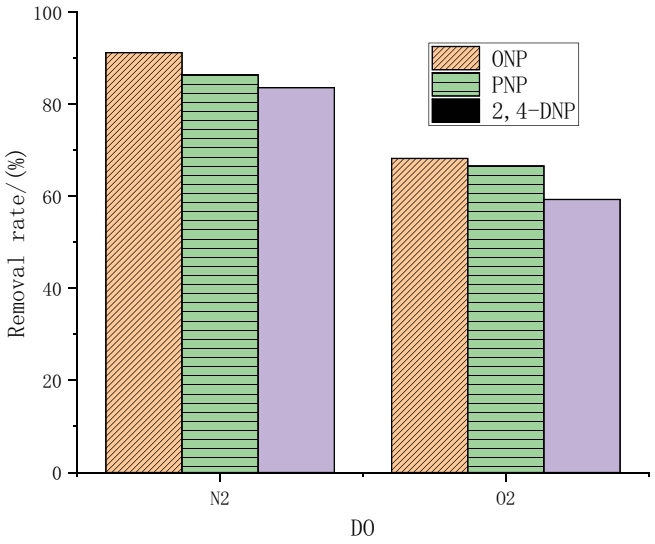

Fig. 12. Effect of dissolved oxygen on nitrophenol removal by nZVI/GAC.

$$Fe + 2H_2O + O_2 \rightarrow Fe^{2+} + 4OH^- \quad (1)$$

As an electron acceptor, oxygen competes with nitrophenol for the active sites on the surface of nano zero-valent iron and the electrons released by nano zero-valent iron, so as to inhibit the reduction of nitrophenol. In the nitrogen system, since there is no oxygen, nano zero-valent iron can react with water as follows:

$$Fe + 2H_2O \rightarrow Fe^{2+} + H_2 + 2OH^- \quad (2)$$

The reasons are as follows: firstly, oxygen competes to use the electrons released by nano zero-valent iron to inhibit the reduction of nitrophenol; Second, the reaction process between oxygen and nano zero-valent iron releases too much OH^- [Eq. (1)], which promotes the formation of iron hydroxide and covers the surface active sites of nano zero-valent iron, so as to greatly reduce the activity of zero-valent iron in reducing nitrophenol.

3.3. Adsorption kinetics analysis

Common adsorption kinetics models mainly include the pseudo-first-order dynamics model and pseudo-second-order dynamics model. The pseudo-first-order dynamics model and pseudo-second-order dynamics model are respectively used to fit the adsorption results of the three materials (GAC, nZVI and nZVI/GAC) to remove ONP, PNP and 2,4-DNP, as shown in Figs. 13 and 14. The dynamic parameters are calculated by the slope and intercept of the curve. The results are shown in Tables 2 and 3.

The pseudo-first-order kinetic model assumes that the adsorption rate of the adsorbent is in direct proportion to the concentration of adsorbate.

$$\log\left(q_e - q_t\right) = \log q_e - \frac{k_1 t}{2.303} \quad (3)$$

In the formula: k_1 is the pseudo-first-rate constant (min^{-1}). Its integral form is:

$$q_t = q_e\left(1 - e^{-k_1 t}\right) \quad (4)$$

The pseudo-second-order kinetic model assumes that the concentration of adsorbate is directly proportional to the square of adsorption speed.

Table 2
Pore structure of GAC and nZVI/GAC materials

Material	Specific surface area (m^2/g)	Pore volume (mL/g)	Aperture (nm)
GAC	961.85	0.4574	2.35
nZVI/GAC	807.58	0.4443	2.26

Table 3
Pseudo-first-order kinetic parameters of different materials for removal of nitrophenols

Sample type		GAC	nZVI	nZVI/GAC
ONP	k_1	0.078	0.032	0.043
	q_e	40.06	11.55	52.24
	R^2	0.951	0.978	0.987
PNP	k_1	0.066	0.025	0.044
	q_e	38.62	11.16	44.93
	R^2	0.967	0.975	0.987
2,4-DNP	k_1	0.059	0.024	0.03
	q_e	35.64	9.69	41.82
	R^2	0.986	0.964	0.991

Table 1
Experimental conditions

Influence factor	Reaction conditions										
nZVI/GAC dosage (g)	0.5	1.5	2.0	2.5	3.0	3.5					
pH	2	3	4	5	6	8	9	10	11		
Reaction time (min)	5	10	15	30	60	120	240	300	360	420	480
Reaction temperature (°C)	20	25	30	35	40						
Initial concentration (mg/L)	50	100	200	300	400	500					

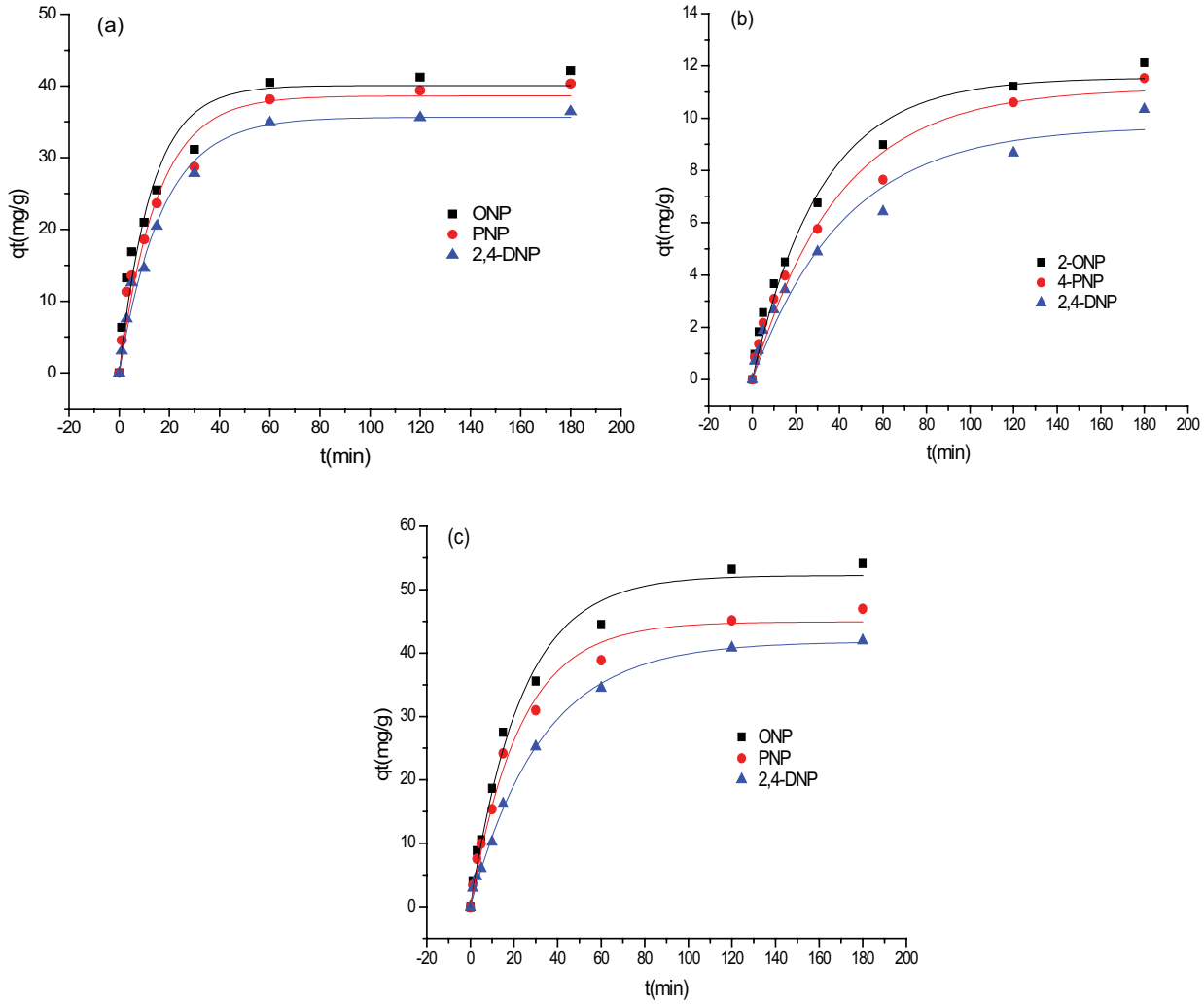

Fig. 13. Fitting curves of pseudo-first-order kinetic equation for nitrophenol removal by different material (a) GAC, (b) nZVI and (c) nZVI/GAC.

$$\frac{t}{q_t}=\frac{1}{k_2 q_e^2}+\frac{t}{q_e} \tag{5}$$

In the formula, k_2 is the pseudo-second-rate constant (g/mg/min).

where q_t and q_e are the adsorption capacity (mg/g) at t time and at equilibrium, respectively.

Its integral expression is:

$$q_t=\frac{tk_2 q_e^2}{1+tk_2 q_e} \tag{6}$$

It can be seen from Tables 3 and 4 that through the comparison of pseudo-first-order kinetics and pseudo-second-order kinetics equation fitting parameters for the removal reaction of three nitrophenols by three different materials, it is found that the correlation coefficient R^2 of pseudo-second-order kinetics equation is more than 0.99, which can better describe the degradation kinetics process. The pseudo-first-order kinetic equation is applicable to describe the adsorption process affected by a single factor or the initial stage of physical adsorption. The pseudo-second-order kinetic equation can be used to describe the adsorption process affected by multiple

Table 4
Pseudo-second-order kinetic parameters for removal of nitrophenols by different materials

Sample type		GAC	nZVI	nZVI/GAC
ONP	k_2	0.0024	0.0025	0.0008
	q_e	44.01	13.81	60.95
	R^2	0.9903	0.9924	0.9963
PNP	k_2	0.002	0.0019	0.0009
	q_e	43.05	13.68	52.37
	R^2	0.9901	0.9889	0.9962
2,4-DNP	k_2	0.0018	0.0021	0.0006
	q_e	40.17	11.94	50.98
	R^2	0.99	0.9830	0.9951

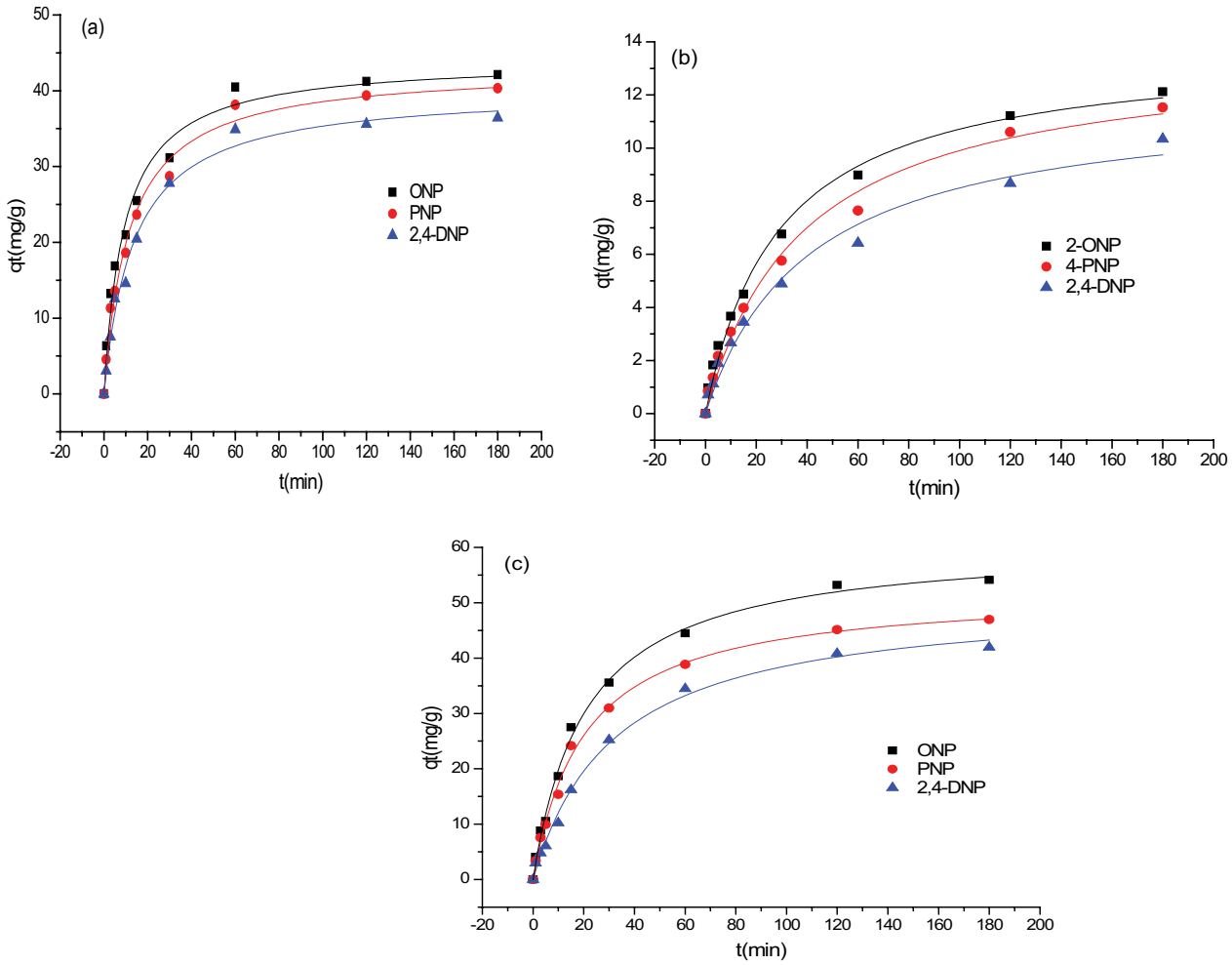

Fig. 14. Fitting curves of pseudo-second-order kinetic equations for nitrophenol removal by different materials (a) GAC, (b) nZVI and (c) nZVI/GAC.

factors and can describe the whole adsorption process such as external liquid film diffusion, particle internal diffusion and surface adsorption, it also shows that there is a chemical reaction in the removal process, and the chemical adsorption mechanism dominates [32].

3.4. Adsorption thermodynamics

Thermodynamic analysis of nitrophenol treated by different materials is helpful to clarify the interaction principle between them. The adsorption isotherms of PNP on GAC, nZVI and nZVI/GAC are analyzed by using the Langmuir model and Freundlich model.

Langmuir formula:

$$q_e = \frac{q_0 K_L C_e}{1 + K_L C_e} \tag{7}$$

Freundlich formula:

$$q_e = K_F C_e^{1/n} \tag{8}$$

In the formula q_e and q_0: the adsorption amount at equilibrium and adsorption amount in the saturated state (mg/g); C_e: the equilibrium concentration (mg/L); K_L, K_F and n: constants.

50 mg of the three materials were respectively weighed and put into 100 mL quantitative flasks. 50 mL of p-nitrophenol solution with different initial concentrations was an addition to each of the three materials and placed in a constant temperature oscillator. Three materials were vibrated in 298 K for 6 h to reach adsorption equilibrium. The adsorption equilibrium was established by 0.45 μ. The concentration of the solution was determined after filtration.

It can be seen from Table 5 that the correlation coefficient of the Freundlich isotherm model is better than that of the Langmuir isotherm model in the thermodynamic analysis of PNP removal by nZVI/GAC, indicating that the adsorption is a multi-molecular layer. The Freundlich constant n exceeds 1, and the range of $1/n$ is between 0 and 1. The closer its value is to zero, the easier it is supposed to be adsorbed by the material. The results show that the three materials are all effective for PNP removal,

and nZVI/GAC has the largest PNP removal n and the smallest $1/n$, indicating that the material has the strongest PNP removal ability.

3.5. Degradation mechanism and path analysis

The comparison of FTIR before and after the degradation of nitrophenol by nZVI/GAC is shown in Fig. 15. The used nZVI/GAC particles show a broad peak at 1,790cm^{-1}, which corresponds to the carbonyl group; it can be seen from Fig. 16 that the peak of Fe^0 in nZVI/GAC

Table 5
Thermodynamic parameters of p-nitrophenol removal by different materials

Materials	Langmuir			Freundlich		
	K_L	q_0	R^2	K_F	n	R^2
GAC	0.056	268.7	0.972	14.25	1.13	0.984
nZVI	0.017	172.7	0.936	2.98	1.06	0.939
nZVI/GAC	0.345	105.35	0.978	31.84	2.23	0.987

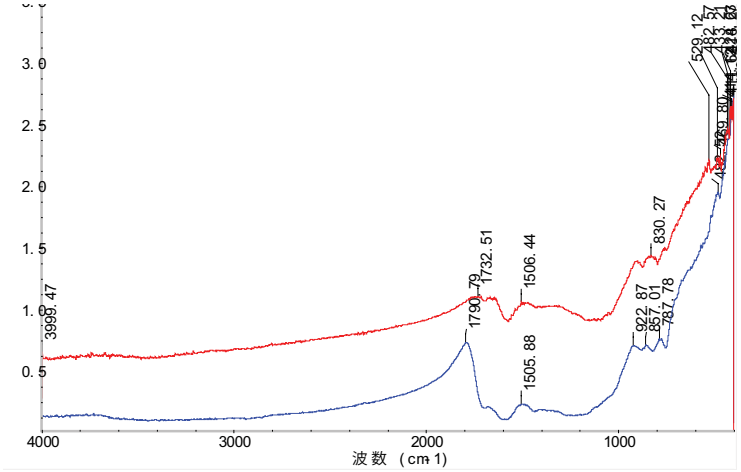

Fig. 15. FTIR spectra of nZVI/GAC particles before and after use.

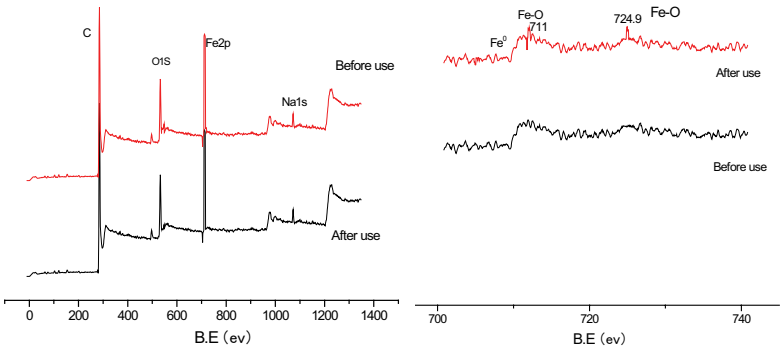

Fig. 16. XPS atlas of nZVI/GAC particles before and after use.

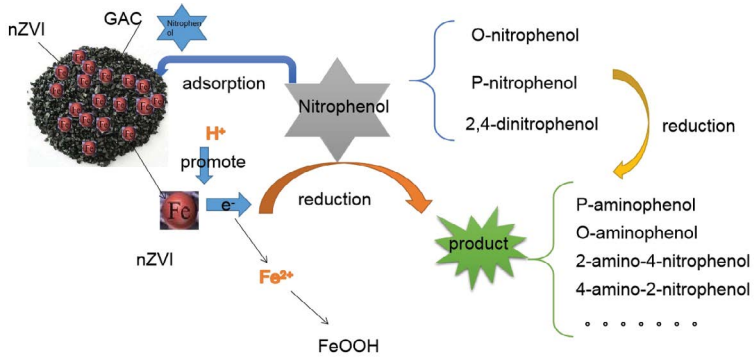

Fig. 17. Mechanism chart of nitrophenol removal by nZVI/GAC.

particles decreases after use, and the peak of iron oxide increases at 711 and 724.9 eV, indicating that zero-valent iron is oxidized after losing electrons. The removal mechanism of nitrophenols by nZVI/GAC is shown in Fig. 17. The removal of nitrophenols is mainly achieved by the synergistic effect of nZVI/GAC adsorption and reduction. The removal mechanism of nitrophenol is that nitrophenol is adsorbed on the surface of activated carbon first under the action of electrostatic attraction, and then is reduced by nano zero-valent iron supported on the surface of activated carbon. The interaction between adsorption and reduction promotes the degradation efficiency of nZVI/GAC.

During the experiment, the products of the solution in the reduction of ONP, PNP and 2,4-DNP by nZVI/GAC were detected by HPLC-MS, as shown in Figs. 18–20.

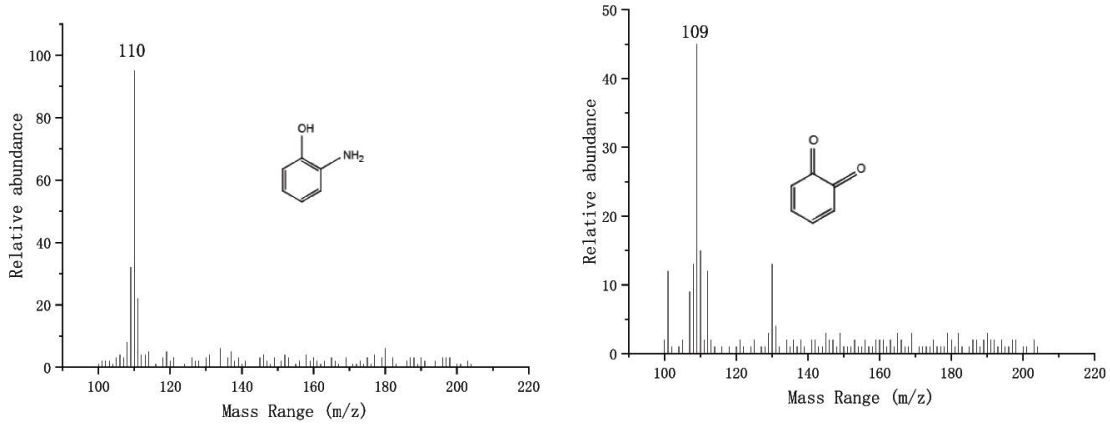

Fig. 18. Analysis of ONP products by high-performance liquid chromatography-mass spectrometry.

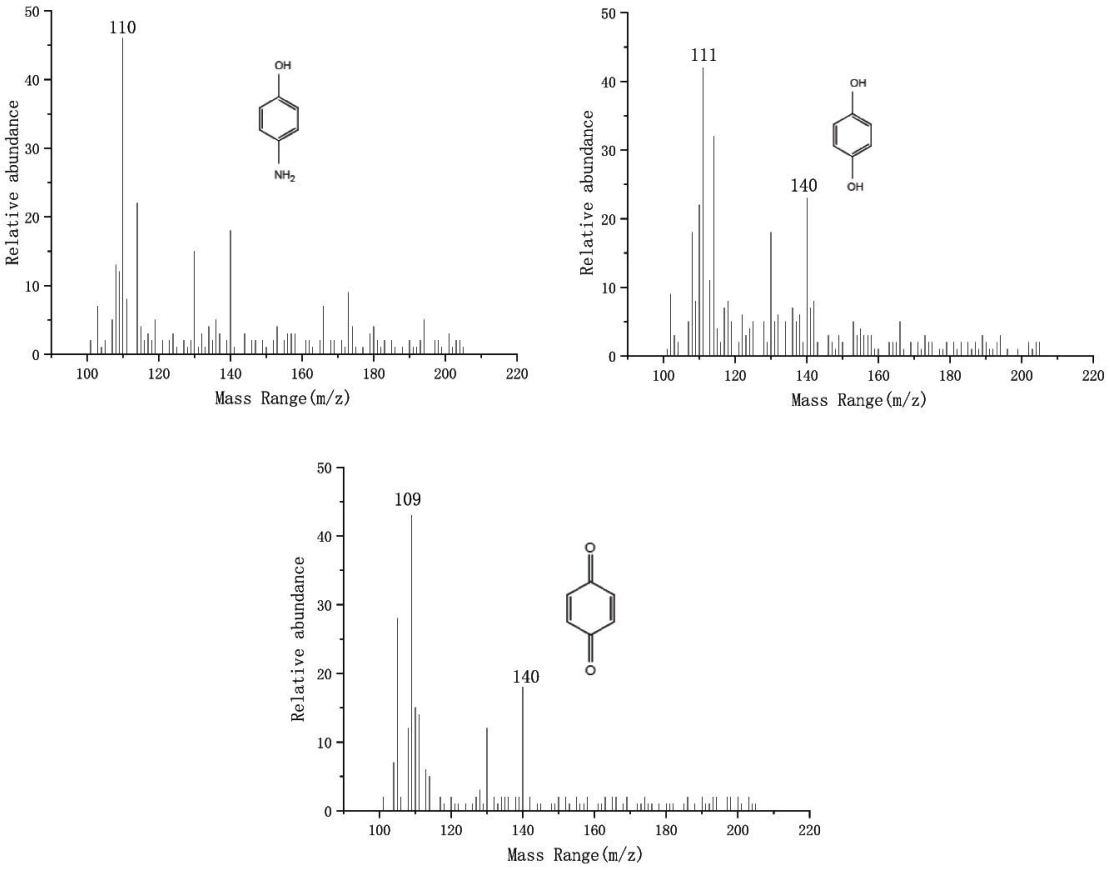

Fig. 19. Analysis of PNP products by high-performance liquid chromatography-mass spectrometry.

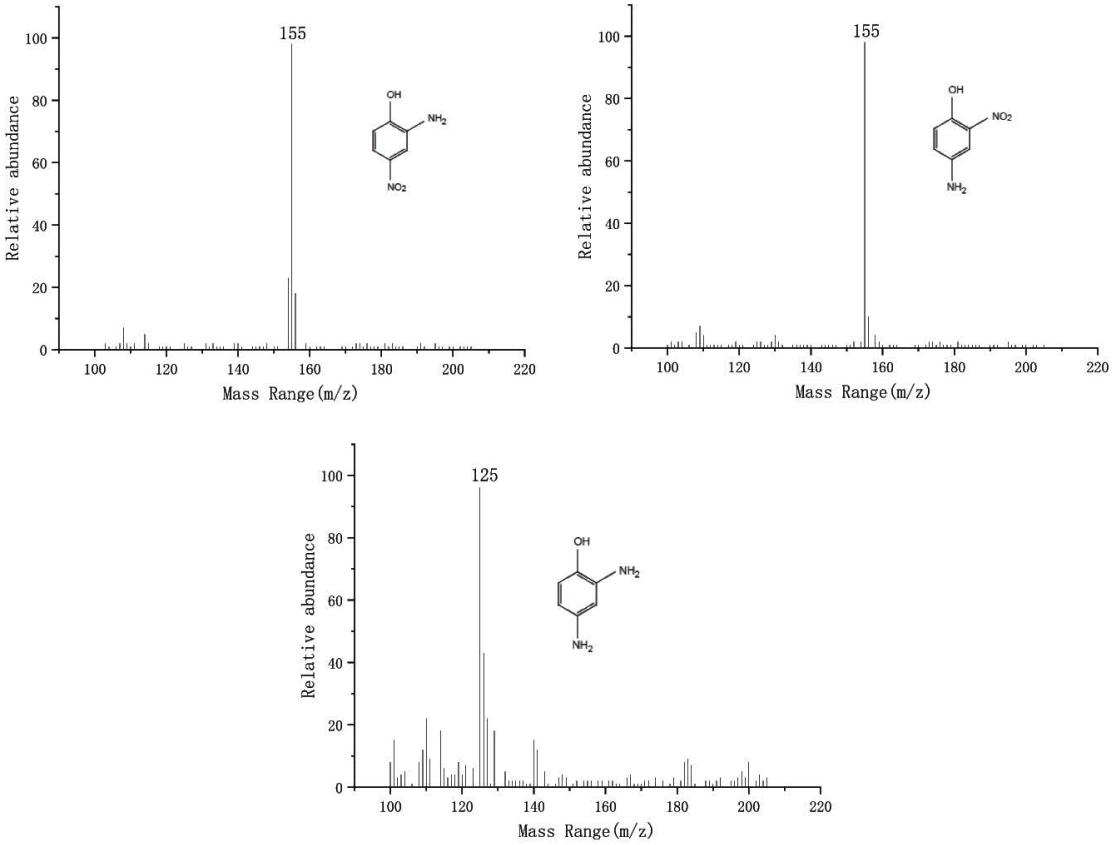

Fig. 20. Analysis of 2,4-DNP products by high-performance liquid chromatography-mass spectrometry.

Through HPLC-MS analysis, combined with the chromatographic peak, and compared with the standard molecular weight of the target compound, Possible compounds of different nitrophenols were preliminarily determined. Main intermediate products of ONP include catechol, o-benzoquinone, o-aniline, etc.; the main intermediate products of PNP include p-aminophenol, p-benzoquinone, p-nitroaniline; the main intermediate products of 2,4-DNP include 2-amino-4-nitrophenol, 4-amino-2-nitrophenol, p-nitrophenol, p-nitro-catechol, o-nitro-hydroquinone, etc.

A possible conversion path is shown in Figs. 21–23.

4. Conclusion

In this work, the nano zero-valent iron supported by granular activated carbon was successfully synthesized, and spherical nano zero-valent iron was uniformly dispersed on the surface of granular activated carbon, which effectively inhibited the aggregation of iron. Under the synergism of adsorption and reduction, the removal rate of nitrophenol was 95% at 30 min. The experimental results showed that the pH of the solution had a greater influence on the removal of nitrophenol, while the reaction temperature had a smaller influence. The removal process of nitrophenol was in line

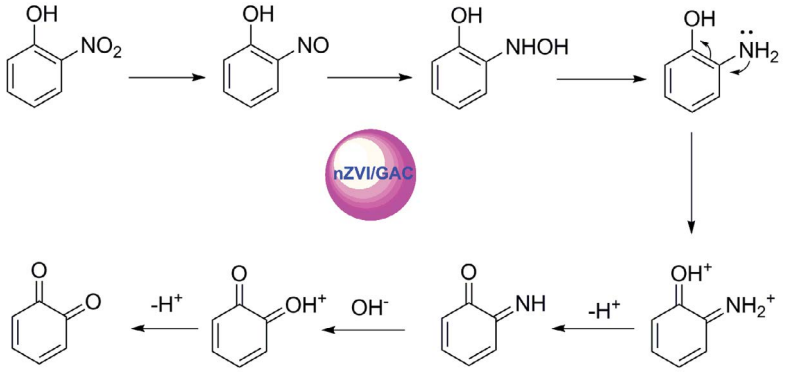

Fig. 21. Degradation pathway of ONP.

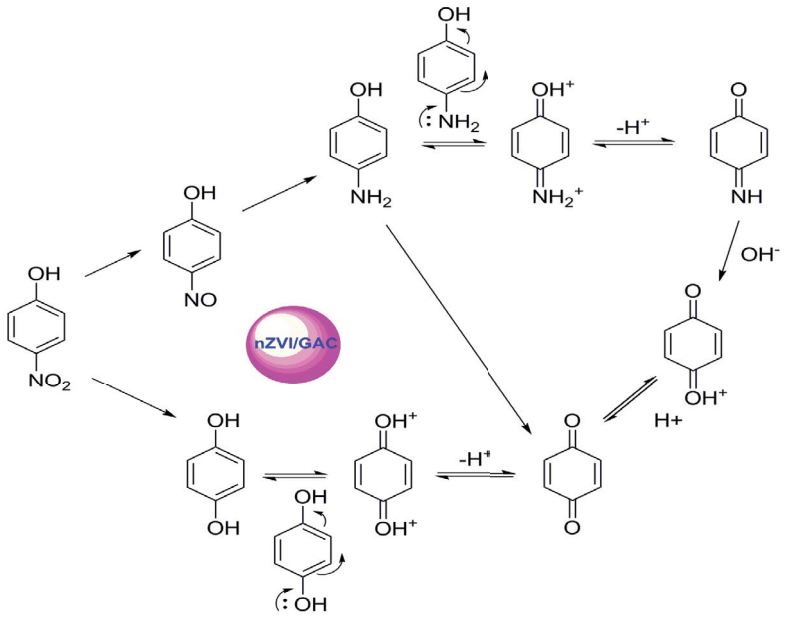

Fig. 22. Degradation pathway of PNP.

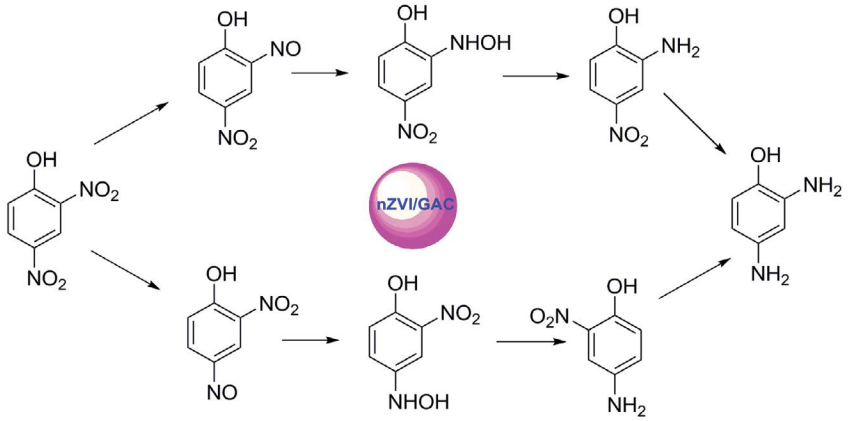

Fig. 23. Degradation pathway of 2,4-DNP.

with the pseudo-second-order reaction kinetics equation. XPS analysis confirmed that the peak of zero-valent iron after nZVI/GAC treatment of nitrophenol decreased. By HPLC-MS intermediate product analysis, the complex can degrade nitrophenolic pollutants into several low-toxic products. Compared with nZVI, the nZVI/GAC composite had better oxidation resistance. Therefore, the above results may provide a suitable method for the removal of nitrophenolic pollutants from water in industrial practice.

Acknowledgments

The study was financially supported by the Jiangsu construction system science and technology project(2019ZD034), supported by the Key Laboratory of Jiangxi Province for Persistent Pollutants Control and Resources Recycle (ES201980193), supported by the National Natural Science Foundation of China (41807368).

References

[1] V. Uberoi, S.K. Bhattacharya, Effects of chlorophenols and nitrophenols on the kinetics of propionate degradation in sulfate-reducing anaerobic systems, Environ. Sci. Technol., 31 (1997) 1607–1614.
[2] Z.K. Xiong, H. Zhang, W.C. Zhang, B. Lai, G. Yao, Removal of nitrophenols and their derivatives by chemical redox: a review, Chem. Eng. J., 359 (2019) 13–31.
[3] R. Das, V.S. Sypu, H.K. Paumo, M. Bhaumik, V. Maharaj, A. Maity, Silver decorated magnetic nanocomposite (Fe_3O_4@PPy-MAA/Ag) as highly active catalyst towards reduction of 4-nitrophenol and toxic organic dyes, Appl. Catal., B, 244 (2018) 546–558.
[4] L.A. Frolova, O.V. Khmelenko, The study of Co–Ni-Mn ferrites for the catalytic decomposition of 4-nitrophenol, Catal. Lett., 151 (2021) 1522–1533.
[5] G.H. Cheng, W. Yu, C. Yang, S.Y. Li, X.Y. Wang, P.Y. Wang, K.G. Zhang, X. Li, G.F. Zhu, Highly selective removal of 2,4-dinitrophenol by a surface imprinted sol–gel polymer, J. Appl. Polym. Sci., 137 (2020) 49236–49246.

[6] K. Shang, W.F. Li, X.J. Wang, N. Lu, N. Jiang, J.L. Li, Y. Wu, Degradation of p-nitrophenol by DBD plasma/Fe^{2+}/persulfate oxidation process, Sep. Purif. Technol., 218 (2019) 106–112.
[7] E.Y. Danish, H.M. Marwani, M.A. Alhazmi, Selectivity and extraction efficiency studies of 4-nitrophenol adsorption on polyethersulfones/Ag nanocomposite, Desal. Water Treat., 67 (2017) 239–246.
[8] M. Zbair, Z. Anfar, H.A. Ahsaine, Reusable bentonite clay: modelling and optimization of hazardous lead and p-nitrophenol adsorption using a response surface methodology approach, RSC Adv., 9 (2019) 5756–5769.
[9] A.A. Babaei, S.N. Alavi, M. Akbarifar, K. Ahmadi, A.R. Esfahani, B. Kakavandi, Experimental and modeling study on adsorption of cationic methylene blue dye onto mesoporous biochars prepared from agrowaste, Desal. Water Treat., 57 (2016) 27199–27212.
[10] A. Azari, B. Kakavandi, R.R. Kalantary, E. Ahmadi, M. Gholami, Z. Torkshavand, M. Azizi, Rapid and efficient magnetically removal of heavy metals by magnetite-activated carbon composite: a statistical design approach, J. Porous Mater., 22 (2015) 1–14.
[11] Y. Guo, M.M. Dai, Z.X. Zhu, Y.Q. Chen, H. He, T.H. Qin, Chitosan modified Cu_2O nanoparticles with high catalytic activity for p-nitrophenol reduction, Appl. Surf. Sci., 480 (2019) 601–610.
[12] S.P. Sam, R. Adnan, S.L. Ng, Statistical optimization of immobilization of activated sludge in PVA/alginate cryogel beads using response surface methodology for p-nitrophenol biodegradation, J. Water Process Eng., 39 (2020) 101725–101738.
[13] Y.Z. Zhou, T. Wang, D. Zhi, B.L. Guo, Applications of nanoscale zero-valent iron and its composites to the removal of antibiotics: a review, J. Mater. Sci., 54 (2019) 12171–12188.
[14] A.A. Babaei, A. Azari, R.R. Kalantary, B. Kakavandi, Enhanced removal of nitrate from water using nZVI@MWCNTs composite: synthesis, kinetics and mechanism of reduction, Water Sci. Technol., 72 (2015) 1988–1999.
[15] S. Li, J.C. Tang, Q.L. Liu, X.M. Liu, B. Gao, A novel stabilized carbon-coated nZVI as heterogeneous persulfate catalyst for enhanced degradation of 4-chlorophenol, Environ. Int., 138 (2020) 105639, doi: 10.1016/j.envint.2020.105639.
[16] M. Stefaniuk, P. Oleszczuk, Y.S. Ok, Review on nano zerovalent iron (nZVI): from synthesis to environmental applications, Chem. Eng. J., 287 (2016) 618–632.
[17] M. Ahmadi, M. Foladivanda, N. Jaafarzadeh, Z. Ramezani, B. Ramavandi, S. Jorfi, B. Kakavandi, Synthesis of chitosan zero-valent iron nanoparticles-supported for cadmium removal: characterization, optimization and modeling approach, J. Water Supply Res. Technol. AQUA, 66 (2017) 116–130.
[18] A. Rostvall, W. Zhang, W.K. Dürig, G. Renman, K. Wiberg, L. Ahrens, P. Gago-Ferrero, Removal of pharmaceuticals, perfluoroalkyl substances and other micropollutants from wastewater using lignite, Xylit, sand, granular activated carbon (GAC) and GAC+Polonite® in column tests – role of physicochemical properties, Water Res., 137 (2018) 97–106.
[19] A.A. Babaei, S.N. Alavi, M. Akbarifar, K. Ahmadi, A.R. Esfahani, B. Kakavandi, Experimental and modeling study on adsorption of cationic methylene blue dye onto mesoporous biochars prepared from agrowaste, Desal. Water Treat., 57 (2016) 27199–27212.
[20] M. Massoudinejad, A. Asadi, M. Vosoughi, M. Gholami, B. Kakavandi, M.A. Karami, A comprehensive study (kinetic, thermodynamic and equilibrium) of arsenic(V) adsorption using $KMnO_4$ modified clinoptilolite, Korean J. Chem. Eng., 32 (2015) 2078–2086.
[21] Y.-H. Hwang, D.G. Kim, H.-S. Shin, Mechanism study of nitrate reduction by nano zero-valent iron, J. Hazard. Mater., 185 (2011) 1513–1521.
[22] T.A. Saleh, Simultaneous adsorptive desulfurization of diesel fuel over bimetallic nanoparticles loaded on activated carbon, J. Cleaner Prod., 172 (2017) 2123–2132.
[23] R.R. Pawar, Lalhmunsiama, M.N. Kim, J.-G. Kim, S.-M. Hong, S.Y. Sawant, S.M. Lee, Efficient removal of hazardous lead, cadmium, and arsenic from aqueous environment by iron oxide modified clay-activated carbon composite beads, Appl. Clay Sci., 162 (2018) 339–350.
[24] M. Kalaruban, P. Loganathan, T.V. Nguyen, T. Nur, Md A.H. Johir, T.H. Nguyen, M.V. Trinh, S. Vigneswaran, Iron-impregnated granular activated carbon for arsenic removal: application to practical column filters, J. Environ. Manage., 239 (2019) 235–243.
[25] Z.T. Li, L. Wang, J. Meng, X.M. Liu, J.M. Xu, F. Wang, P. Brookes, Zeolite-supported nanoscale zero-valent iron: new findings on simultaneous adsorption of Cd(II), Pb(II), and As(III) in aqueous solution and soil, J. Hazard. Mater., 344 (2017) 1–11.
[26] X. Shang, L. Yang, D. Ouyang, B. Zhang, W.Y. Zhang, M.Y. Gu, J. Li, M.F. Chen, L.H. Huang, L.B. Qian, Enhanced removal of 1,2,4-trichlorobenzene by modified biochar supported nanoscale zero-valent iron and palladium, Chemosphere, 249 (2020) 126518, doi: 10.1016/j.chemosphere.2020.126518.
[27] Y.C. Lv, S.Y. Huang, G.F. Huang, Y.F. Liu, G.F. Yang, C.X. Lin, G. Xiao, Y.H. Wang, M.H. Liu, Remediation of organic arsenic contaminants with heterogeneous Fenton process mediated by SiO_2-coated nano zero-valent iron, Environ. Sci. Pollut. Res., 27 (2020) 12017–12029.
[28] D. Dong, R.K. Wang, P.F. Geng, C.X. Li, Z.H. Zhao, Enhancing effects of activated carbon supported nano zero-valent iron on anaerobic digestion of phenol-containing organic wastewater, J. Environ. Manage., 244 (2019) 1–12.
[29] P.D. Mines, B. Uthuppu, D. Thirion, M.H. Jakobsen, C.T. Yavuz, H.R. Andersen, Y. Hwang, granular activated carbon with grafted nanoporous polymer enhances nanoscale zero-valent iron impregnation and water contaminant removal, Chem. Eng. J., 339 (2018) 22–31.
[30] J.S. Lee, W.Y. Choi, J.Y. Yoon, Photocatalytic degradation of N-nitrosodimethylamine: mechanism, product distribution, and TiO_2 surface modification, Environ. Sci. Technol., 39 (2005) 6800–6807.
[31] Q.Q. Jin, S. Zhang, T. Wen, J. Wang, P.C. Gu, G.X. Zhao, X.X. Wang, Z.S. Chen, T. Hayat, X.K. Wang, Simultaneous adsorption and oxidative degradation of Bisphenol A by zero-valent iron/iron carbide nanoparticles encapsulated in N-doped carbon matrix, Environ. Pollut., 243 (2018) 218–227.
[32] H. Qiu, L. Lv, B.-C. Pan, Q.-J. Zhang, W.-M. Zhang, Q.-X. Zhang, Critical review in adsorption kinetic models, J. Zhejiang Univ.-Sci. A, 5 (2009) 716–724.